Performance and economic assessment of enriched gadolinia burnable absorbers

Bolukbasi, Mustafa; Middleburgh, Simon; Dahlfors, Marcus; Lee, Bill

Progress in Nuclear Energy

DOI:
https://doi.org/10.1016/j.pnucene.2021.103752

Published: 01/07/2021

Peer reviewed version

Performance and economic assessment of enriched gadolinia burnable absorbers

M.J. Bolukbasi[1], S.C. Middleburgh[1], M. Dahlfors[1], W.E. Lee[1,2]
[1.] *Nuclear Futures Institute, Bangor University, Bangor, LL57 1UT, U.K.*
[2.] *Department of Materials, Imperial College London, London, SW7 2AB, U.K.*

Abstract

As a burnable absorber, gadolinium oxide (Gd_2O_3) is widely used in light water reactors due to the high neutron absorption cross section of several gadolinium isotopes and its good solid solubility in UO_2. However, some isotopes of natural Gd cause residual reactivity suppression, while some are not efficient neutron absorbers, reducing the efficiency of the burnable absorber when implemented. In this study, fuel assemblies utilising gadolinium oxide enriched with ^{157}Gd isotope were modelled using Monte Carlo particle transport methods and compared to fuel with a natural Gd based absorber. Reactivity gains were examined over the life of the assembly utilising ^{157}Gd-enriched absorber as compared to natural gadolinia. A preliminary economic evaluation is also made to assess the commercial benefits of using ^{157}Gd-enriched burnable absorber. Use of enriched gadolinium oxide is shown to eliminate residual reactivity caused by natural gadolinium oxide, and similar reactivity properties (and therefore criticality margins) can be achieved with less burnable absorber in the fuel. The financial cost of incorporating enriched Gd isotopes into nuclear fuel has also been estimated.

Keywords**:** Gadolinium oxide, Enriched gadolinium, Burnable absorber, Monte Carlo.

1. Introduction

Nuclear fuel assembly design is generally optimised to support the economical operation of a reactor, enabling it to reach the highest possible capacity factor. To achieve best economic performance, it is typically necessary to operate for as long a period as possible between refuelling operations or outages. Extending the fuel cycle in this way will increase the total amount of power produced and thus minimise the number of outage days during the reactor lifetime (Ozer and Edsinger, 2006). The longer fuel cycle length requires a combination of improvements to the fuel, including loading a higher fuel enrichment (Durazzo *et al.*, 2018) or higher uranium density fuel, for example through the Advanced Technology Fuel (ATF) developments (Middleburgh *et al.*, 2020). As a result of the higher enrichment/higher U density, a range of reactivity suppression methods can be employed to ensure the safety margins are maintained and the reactor is controllable when the fuel is fresh (Galahom, 2017).

Burnable absorbers (BAs) represent one such method to suppress the reactivity of fresh fuel (Frybortova, 2019), preventing excessively high power peaks (Tran *et al.*, 2017). They effectively capture neutrons and in doing so they transmute to isotopes with lower neutron cross sections (i.e. they are burned) enabling the fuel to be efficiently used thereafter. In addition, the most ideal burnable absorbers are those that do not leave any residual absorption in the system after their burn (Santala *et al.*, 1997).

Gadolinium oxide (Gd_2O_3) is one of the most regularly employed burnable absorbers because of the high neutron capture cross section of gadolinium isotopes (Uguru *et al.*, 2020). It is used in a limited number of fuel rods to prolong suppression and take advantage of self-shielding effects (Franceschini and Petrović, 2009). Gadolinium provides a means to control the power peak within the assembly and has relatively little impact on the reprocessing of the fuel (Schlieck *et al.*, 2001).

Fig. 1 shows the infinite multiplication constant (k_{inf}) of fuel assemblies, which is a measure of their ability to generate power, that have been enriched with 5 wt.% ^{235}U and contain 1.00 wt.%, 2.00 wt.% 4.00 wt.%

and 6.00 wt.% n-Gd_2O_3 (Gd_2O_3 with a natural abundance of its isotopes). The methodology used in obtaining this graph is given in section 2. Although reactivity in the PWR assembly without BA shows a steady decrease, in assemblies that contain BA in the form of n-Gd_2O_3, the reactivity first rises and reaches a maximum level at the point where BA is almost depleted. The point at which k_{inf} is highest is referred to as the "peak reactivity". The k_{inf} subsequently decreases steadily in parallel with the assembly without BA (Sanders and Wagner, 2002). It can be seen that assemblies with more burnable absorber have a reduced k_{inf} at the end of cycle due to residual suppression by the additives.

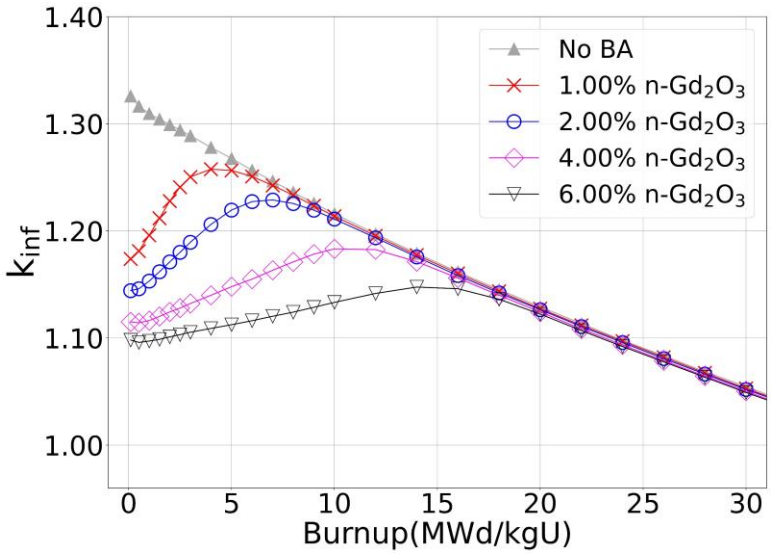

Fig. 1 Infinite multiplication constant (k_{inf}) at 5% ^{235}U enrichment level and containing 1.00 wt.%, 2.00 wt.%, 4.00 wt.% and 6.00 wt.% n-Gd_2O_3. Increasing Gd_2O_3 content suppresses peak point reactivity.

When n-Gd_2O_3 is used as BA, the isotopes having low thermal neutron absorption cross section impact negatively on reactivity, causing residual absorption in later life (Franceschini and Petrović, 2009). It is possible to negate this negative effect by enriching Gd_2O_3 with ^{157}Gd, the most efficient neutron absorbing Gd isotope (Santala *et al.*, 1997). As this enrichment process allows reduction of the amount of Gd_2O_3 to be used in the fuel pellets, it helps to decrease the negative effect of Gd_2O_3 on pellet thermal conductivity (Dalle *et al.*, 2013; Qin *et al.*, 2020), which in turn may help to reduce or entirely remove the penalties traditionally imposed on the Thermo-Mechanical Operating Limit (TMOL) for Gd fuel rods. It also reduces the overall uranium oxide (UO_2) displacement in the fuel matrix (Yilmaz, 2005) so that a higher UO_2 loading is obtained in the assembly.

Natural Gd contains seven stable isotopes: ^{155}Gd (14.80%) and ^{157}Gd (15.65%) are the isotopes with the highest neutron absorption cross sections : 61,000±500 barns and 254,000±2000 barns, respectively (Oprea and Oprea, 2014). When ^{157}Gd captures a neutron that would have otherwise initiated a fission event, it transmutes to ^{158}Gd that has a significantly lower neutron cross section and has thus "burned" away. However, when ^{156}Gd (~20 wt.% of the natural abundance of Gd and the product of neutron capture of ^{155}Gd) absorbs a neutron, it produces ^{157}Gd (the efficient absorber). This production of neutron absorbing isotopes reduces the efficiency of the burnout of the burnable absorber causing residual reactivity suppression. Another absorber regularly used in fuel: ^{10}B (often in the form of ZrB_2 (Simmons *et al.*, 1988)) absorbs a neutron and breaks down into two low neutron absorbing isotopes: ^4He and ^7Li – however the efficiency of neutron capture by ^{10}B is lower than ^{157}Gd and incorporation of boron into the fuel matrix has also been an engineering challenge. The oxide of boron, B_2O_3, when in UO_2 solution causes poor properties of the pellet and its volatility during sintering makes commercial production extremely challenging. Other boron containing compounds and boron composites are being researched at present(Kardoulaki et al., 2020) and ZrB_2 coatings have been applied to pellets(Franceschini and Petrović, 2009), avoiding many chemical compatibility issues.

Bejmer and Seveborn investigated the effect of Gd_2O_3 enriched with 70% ^{157}Gd in the Westinghouse 3-loop pressure water reactor and suggested that e-Gd_2O_3(Gd_2O_3 enriched in ^{157}Gd) did not have any

negative effects in the core and extended the fuel cycle length (Bejmer and Seveborn, 2004). Dalle and others (Dalle *et al.*, 2013) performed simulations using e-Gd_2O_3 at different weight percentages in the fuel composition and determined that the e-Gd_2O_3 provides an increased and more stable reactivity in late life fuel compared to n-Gd_2O_3. Yilmaz *et al.* replaced n-Gd_2O_3 with the same amount of e-Gd_2O_3. They showed that the same reactivity behaviour in the core can be provided with a lower rate of ^{235}U enrichment, and thus, they stated that savings in fuel costs can be achieved (Yilmaz *et al.*, 2006).

For a nuclear reactor, it is economically advantageous to load fuel with the highest reactivity potential into the reactor core – within given safety margins, so that the fuel cycle cost can be saved by running the reactor longer(Galahom, 2016). The fuel cycle length can be extended using e-Gd_2O_3, due to the reactivity-enhancing effect obtained (Schlieck, Berger and Neufert, 2001). The enrichment process with ^{157}Gd could be performed with traditional techniques (Santala *et al.*, 1997), but the high cost of these techniques made the BA cost of fuel more expensive than the fuel itself (Renier and Grossbeck, 2001). For instance, the cost of magnetic separation with calutron was $1000 per gram of Gd however this cost has been reduced using new techniques such as PSP (plasma separation process) (Renier and Grossbeck, 2001). Yilmaz determined that the cost of ^{157}Gd enrichment with PSP is less than 10 dollars gram/^{157}Gd (Yilmaz, 2005).

This study investigates the reactivity properties of e-Gd_2O_3 BA that can be obtained by enriching Gd_2O_3 with ^{157}Gd isotopes to eliminate the residual reactivity caused by n-Gd_2O_3, and furthermore estimates the financial implications related to assembly cost when incorporating e-Gd_2O_3.

2. Method

2.1. Reactor and fuel modelling

The Serpent 2 Monte Carlo reactor physics code, developed by VTT Technical Research Centre, was used throughout this study (Leppänen *et al.*, 2015). The reactor and assembly level simulation parameters used in the study are shown in Table 1. In this study, it was assumed that the e-Gd_2O_3, contains 100 wt.% ^{157}Gd isotopes after the enrichment process (although it is noted that any enrichment process is likely to leave impurity isotopes) in order to assess the maximum impact of using e-Gd_2O_3 versus n-Gd_2O_3.

Table 1. Parameters used in Serpent 2 simulations.

Reactor Type	PWR
Number of BA rods	24
Fuel temperature (K)	900
Cladding Temperature (K)	583
Fuel density	95%
Neutron population (neutrons per cycle)	30000
Cycles (active/ inactive)	300 / 20

A range of simulations were carried out to identify designs where n-Gd_2O_3 and e-Gd_2O_3 show similar reactivity characteristics (matching both k_{inf} and the burnup at which the peak point reactivity occurs). The enrichment of ^{235}U considered throughout the paper ranges from 3 wt.% to 6%, capturing some potential effects of extending the commercially available enrichment for light water reactors to beyond 5 wt.%. Fuel densities of the models mentioned in this paper were calculated by using data from (IAEA, 1995) and are provided in appendix Table A1.

2.2 Reference fuel design

This study was based on the AP-1000 PWR reactor designed by Westinghouse Electric Company and some of its features used while creating the fuel designs in this study are given in Table 2 (Nuclear Regulatory Commission, 2011). The design of the fuel assembly is based on two reference assemblies (see Appendix Fig. A1 and Fig. A2). Although both of the assemblies contain 24 BA rods and 25 control rods, the placement of BA rods differs within the assemblies. The designs of the rods (see Appendix Fig

A3) is the same for both assemblies. While the fuel in regular rods was UO_2, BA rods had different proportions of Gd_2O_3 addition as well as UO_2.

Table 2. Fuel design parameters of AP-1000 PWR reactor.

Rod array	17×17
Number of control rods	25
Fuel rod pitch (cm)	1.26
Pellet diameter(cm)	0.819
Rod diameter (cm)	0.949
Cladding material	Zircaloy 4
Cladding thickness(cm)	0.057

Due to self-shielding effects, it is known that the Gd atoms in the outer layer of the fuel pellet will transmute more rapidly than inner layer as they will absorb neutrons moderated by the coolant water, shielding the gadolinium atoms in the inner portions of the pellet (Pagano *et al.*, 2008). To observe the depletion behaviour of the Gd isotopes in the fuel pellets as a function of radius, the concentration of Gd isotopes in 11 radial layers of equal volume, from the centre of the fuel pellet to the surface was investigated. This method was also carried out to observe changes in ^{239}Pu breeding. In the study, the reactivity error margins observed for all models varied between approximately 15 to 21 pcm (1 pcm = 10^{-5}), too small to be of consequence to our results.

2.3 Cost calculations

Calculation of the fuel cycle cost is made by considering the unit costs of all components within the cycle. In addition to the performance related calculations, the economic impact of using e-Gd_2O_3 is investigated in terms of its impact on assembly cost by considering the uranium purchase, conversion, enrichment, and fabrication costs.

In calculations, unit prices were calculated to be low, medium, and high to reflect uncertain fluctuations in unit costs that may occur (Ko and Gao, 2012) and unit costs taken from the literature for these calculations are given in appendix Table A2. The calculation of fuel cost formulas as specified by OECD / NEA were used in this study (*The Economics of the Nuclear Fuel Cycle*, 1994) with updated values. An example of the formula used to calculate the cost of each item is given in Eq.1. In this formula, X_i is the amount of product processed, f_i is loss factor of operation, P_i is the per unit cost, S_i is the escalation rate, t is time and t_b is the base date of monetary unit.

$$F_i = X_i \times f_i \times P_i \times (1 + S_i)^{t-t_b} \qquad \text{(Eq. 1)}$$

On the other hand, ^{157}Gd enrichment cost was calculated with the Eq. 2 (Yilmaz, 2005) while the purchase cost of BA, was calculated with the Eq. 3. The purchase cost of BA was not included to the fuel fabrication cost and was calculated as a separate item in order to show the difference between n-Gd_2O_3 and e-Gd_2O_3 more clearly.

$$F_{Gd\ enrichment} = M_{Gd} \times P_{en} \times 1000 \qquad \text{(Eq. 2)}$$

$$F_{\text{Gd purchasing}} = M_{Gd} \times P_{Gd} \qquad \text{(Eq. 3)}$$

Where M_{Gd} is the mass of Gd_2O_3 used in assembly, P_{en} is the ^{157}Gd enrichment cost of per gram Gd_2O_3, and P_{Gd} is the purchase cost of per kilogram Gd_2O_3.

The total cost of fuel per assembly is obtained by summing each cost item. All formulae related to cost calculations can be found in Appendix A. In addition, while the parameters of the formulas are given in

appendix Table A3, the fuel cycle data required for the calculation of costs are given in appendix Table A4.

3. Results and discussion

3.1. Assembly design and ^{235}U enrichment

Fig. 2 shows the k_{inf} of different n-Gd_2O_3 additions to the two assembly designs A1 and A2 highlighting that small changes in the location of the BA rods within the fuel assembly do not cause a significant effect on the overall reactivity behaviour within the assembly. As expected, the larger addition of n-Gd_2O_3 causes a larger suppression in k_{inf} and also shifts the peak point reactivity towards higher burnups. As a result of these behavioural trends, all subsequent simulations were performed using the A1 assembly layout.

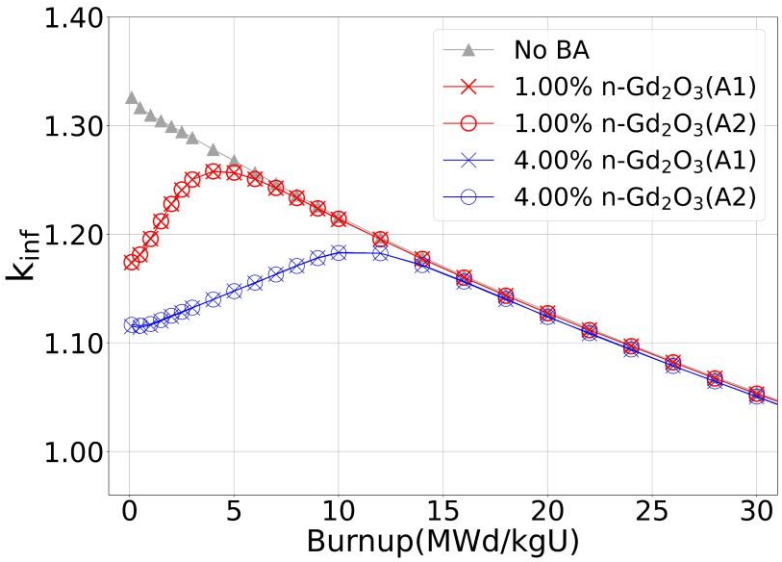

Fig. 2 Infinite multiplication constant (k_{inf}) for 5 wt.% ^{235}U with no BA, and 1.00 wt.%, and 4.00 wt.% n-Gd_2O_3 in two different assembly layouts (A1 and A2).

Fig. 3 shows the multiplication factor (k_{inf}) trends in models with different ^{235}U enrichment levels in assembly A1 (with 2.00 wt.% n-Gd_2O_3 BA rods). As expected, the total reactivity increases due to the increasing ^{235}U content. For each enrichment value, BA-containing models have a lower multiplication factors at the beginning of cycle (i.e. they are suppressed). As burnup proceeds, the multiplication factor rises until the ^{155}Gd and ^{157}Gd isotopes are mostly depleted (see Fig A4). With the depletion of these isotopes, the full fissile content of the assembly is exposed and begins depleting with multiplication factors of the assemblies declining again in close proximity to the reactivity curve of the reference model without BA additions.

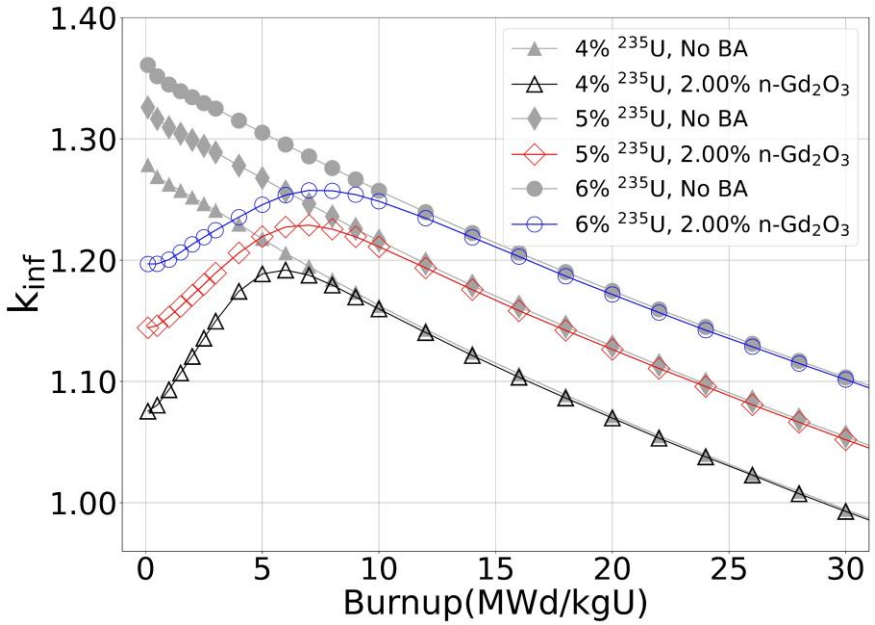

Fig. 3 Burnup behaviour of models containing 4 wt.%, 5 wt.% and 6 wt.% ^{235}U and 2.00 wt.% Gd_2O_3 and their reference models without BA.

It is also noticeable that after the depletion of Gd isotopes (i.e. beyond ~10 MWd/kgU), there is a slight decrease in the reactivity of BA using assemblies compared to those without BA – this is the residual reactivity suppression. In addition, because ^{235}U is also a neutron absorber, with increasing concentration of ^{235}U in the fuel composition, the depletion of Gd isotopes is delayed and these results agree with those of Dalle and others (Dalle *et al.*, 2013). For all subsequent calculations in the main body of this article, 5 wt.% ^{235}U enrichment of the UO_2 is utilized as the general behaviour is expected to be similar.

Simulations were performed to investigate the differences in reactivity behaviour occurring when equal amounts of n-Gd_2O_3 and e-Gd_2O_3 are used in BA rods. Fig. 4 compares reactivity behaviour of model fuels with 1.00 wt.% of n-Gd_2O_3 and 1.00 wt.% of e-Gd_2O_3, both with 5 wt.% ^{235}U enrichment. As can be seen, the reactivity is suppressed in the e-Gd_2O_3 and flattened compared to that with n-Gd_2O_3 addition. The cause of this behaviour can be traced to the greater amount of ^{157}Gd in the e-Gd_2O_3 assembly. Also, the burn of ^{155}Gd in the n-Gd_2O_3 pellet burns away more slowly compared to ^{157}Gd (see Fig. A4), a result of the lower neutron capture cross section. The suppression of the reactivity in the e-Gd_2O_3 assembly is significantly stronger and remains absorbing for longer than when n-Gd_2O_3 is used, results that are in agreement with (Renier and Grossbeck, 2001).

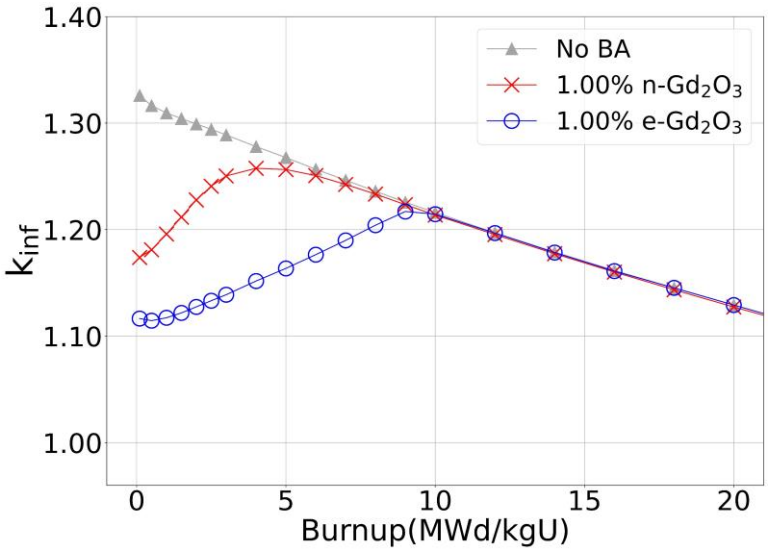

Fig. 4 Infinite multiplication constant (k_{inf}) as a function of burnup for model fuels with 5 wt.% ^{235}U and 1.00 wt.% n-Gd_2O_3, 5 wt.% ^{235}U and 1.00 wt.% e-Gd_2O_3, and fuel model with 5 wt.% ^{235}U and without BA.

Based on these results, we now investigate how a lower amount of e-Gd_2O_3 can be utilized to provide a similar (or enhanced) reactivity suppression compared to n-Gd_2O_3.

3.2. Comparison natural Gd_2O_3 and enriched Gd_2O_3 showing similar reactivity behaviours

3.2.1. Reactivity behaviour

Three matches with similar peak reactivity behaviour (Fig. 5a, 5b and 5c) and another three matches with equal highest reactivity rates (Fig 5d, 5e and 5f) for n-Gd_2O_3 and e-Gd_2O_3 in fuels were identified and further examined.

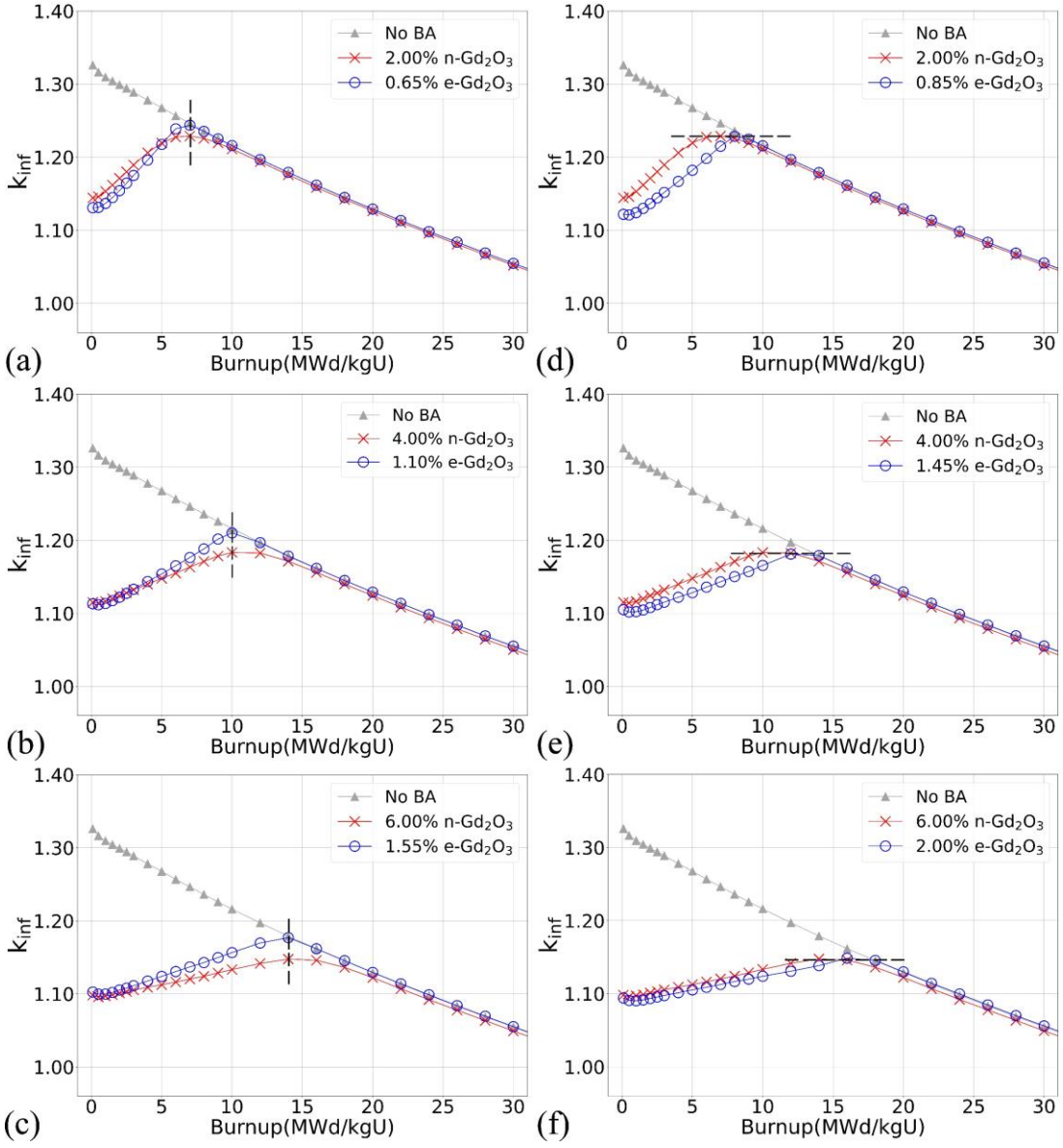

Fig. 5. Infinite multiplication constant for (a) 2.00 wt.% n-Gd_2O_3, and 0.65 wt.% e-Gd_2O_3, (b) 4.00 wt.% n-Gd_2O_3, and 1.10 wt.% e-Gd_2O_3, (c) 6.00 wt.% n-Gd_2O_3, and 1.55 wt.% e-Gd_2O_3 (d) 2.00 wt.% n-Gd_2O_3, and 0.85 wt.% e-Gd_2O_3, (e) 4.00 wt.% n-Gd_2O_3, and 1.45 wt.% e-Gd_2O_3 (f) 6.00 wt.% n-Gd_2O_3, and 2.00 wt.% e-Gd_2O_3.

When designs with similar peak reactivity behaviour (Fig. 5a, 5b and 5c) are examined, assemblies where e-Gd_2O_3 was used are more suppressed at the beginning of the cycle for the two lower Gd contents considered (Figs. 5a and 5b). From low-to-intermediate burnups (~5MWd/kgU), e-Gd_2O_3 provides a higher reactivity compared to the n-Gd_2O_3 for the rest of the cycle. Of significance, for the composition

containing the highest e-Gd_2O_3 content (Fig. 5c), the e-Gd_2O_3 assembly provided a higher reactivity than n-Gd_2O_3 throughout the cycle.

In Figures 5a-5c, assemblies with e-Gd_2O_3 have higher peak k_{inf} values than models having n-Gd_2O_3 and then follow the no-BA k_{inf} values efficiently for the rest of the operation. The increase in k_{inf} can be explained by two important factors for these matching models: (1) an absence of Gd isotopes that have low neutron absorption cross-section but transmute and cause residual reactivity in the composition of e-Gd_2O_3; (2) use of lower amounts of Gd_2O_3 when utilizing e-Gd_2O_3, which reduces the BA percentage in the fuel composition, to achieve a similar reactivity behaviour to n-Gd_2O_3, thus resulting in a lower amount of UO_2 displacement.

On the other hand, when designs with equal highest reactivity rates are examined in Figs. 5d-5f, assemblies incorporating e-Gd_2O_3 suppress the reactivity more than n-Gd_2O_3 from the beginning of the cycle until the Gd isotopes are completely depleted in the assembly. However, e-Gd_2O_3 provides higher reactivity in the rest of the cycle (beyond the BA burn-out). This increase in the rest of the cycle can be explained by the absence of isotopes in the fuel composition that causes residual reactivity and the higher fissile U loading due to the use of lower volume of BA, as also observed in models with matching peak reactivity behaviour.

The reactivity differences (Δk_{inf}) between the models with n-Gd_2O_3 and e-Gd_2O_3 in Fig. 5 are reported in Fig. 6, in units of pcm. As noted earlier, the e-Gd_2O_3 reactivity is suppressed compared to n-Gd_2O_3 during early stages of irradiation. To calculate the difference that e-Gd_2O_3 will cause on the total reactivity, accumulated reactivity gain for each match also was computed (see Fig. A5). For matching of similar peak reactivity behaviours, the use of e-Gd_2O_3 provides a higher total reactivity gain than the amount reduced at the beginning of life in the matches reported in Fig. 5a (2.00 wt.% n-Gd_2O_3 and 0.65 wt.% e-Gd_2O_3) and Fig. 5b (4.00 wt.% n-Gd_2O_3 and 1.10 wt.% e-Gd_2O_3). The assemblies shown in Fig 5c (6.00 wt.% n-Gd_2O_3 compared to 1.55 wt.% e-Gd_2O_3) show a reactivity benefit from the beginning of life. These values indicate that the comparative benefit of reactivity increases with increasing amount of burnable absorber added to the assembly.

On the other hand, in the matches reported in Figures 5d and 5e, with equal highest reactivity rates, e-Gd_2O_3 reduces the reactivity at the beginning of the cycle more than the gain in k_{inf} provided at the late of the cycle. The situation changes in Figure 5f, and e-Gd_2O_3 provides a higher reactivity gain in the rest of the cycle than the amount reduced at the beginning of the cycle. This will have a subsequent impact on the cost of an assembly (see Section 3.4).

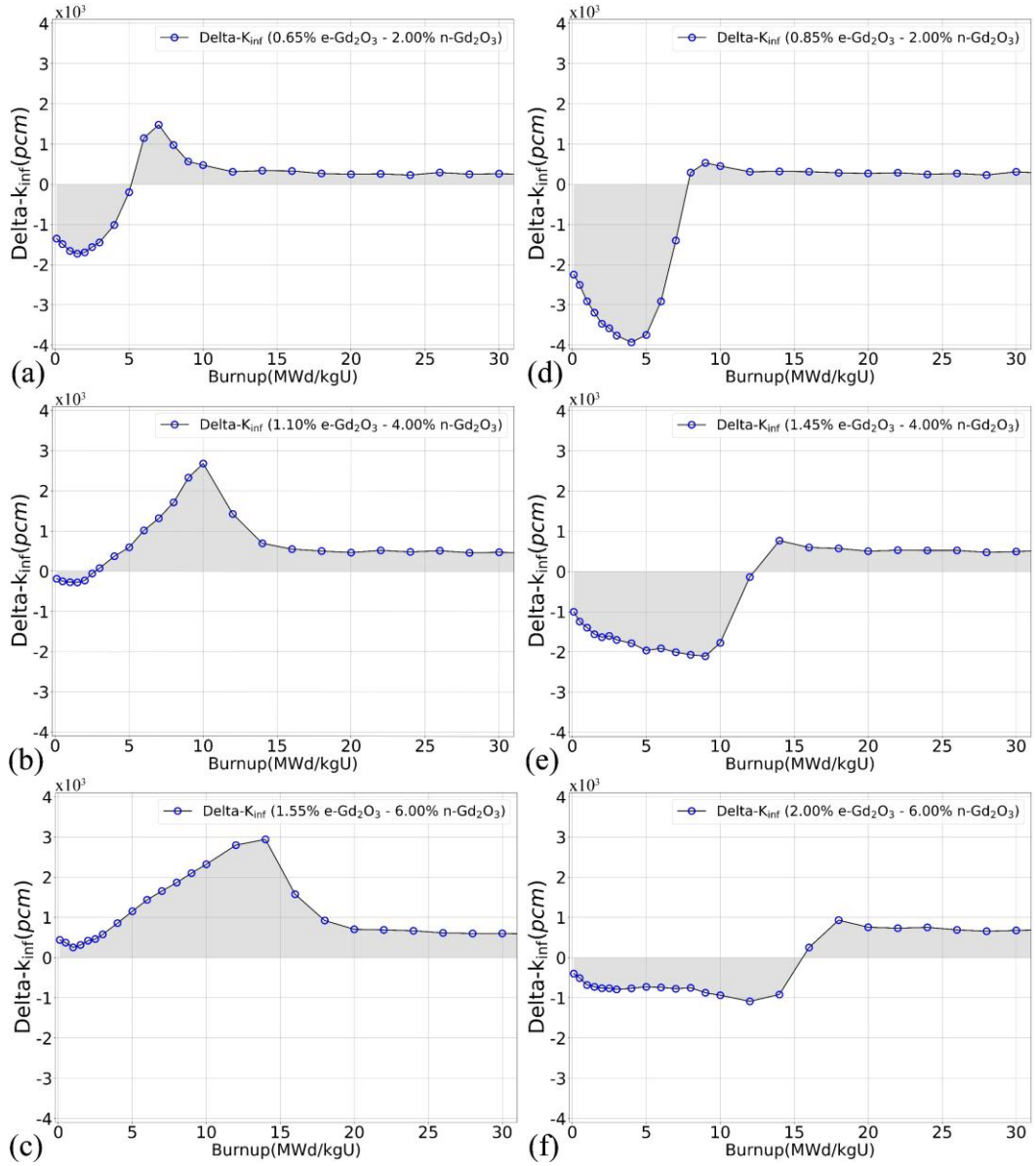

Fig. 6 Delta-k_{inf} for (a) 2.00 wt.% n-Gd_2O_3, and 0.65 wt.% e-Gd_2O_3, (b) 4.00 wt.% n-Gd_2O_3, and 1.10 wt.% e-Gd_2O_3, (c) 6.00 wt.% n-Gd_2O_3, and 1.55 wt.% e-Gd_2O_3, (d) 2.00 wt.% n-Gd_2O_3, and 0.85 wt.% e-Gd_2O_3, (e) 4.00 wt.% n-Gd_2O_3, and 1.45 wt.% e-Gd_2O_3, (f) 6.00 wt.% n-Gd_2O_3, and 2.00 wt.% e- Gd_2O_3

Fig. 7 summarises the patterns obtained after similar reactivity characteristics (similar peak reactivity behaviours and equal highest reactivity rates) were detected in the investigation of models containing 1.00 to 6.00 wt.% n-Gd_2O_3 and 0.30 to 2.00 wt.% e-Gd_2O_3 in 3 wt.%, 4 wt.% 5% and 6 wt.% UO_2 fuel.

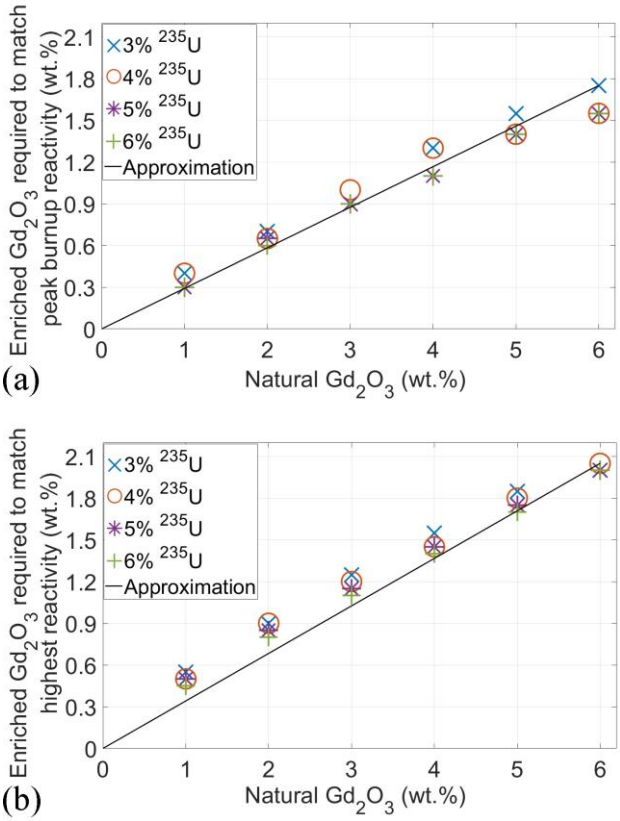

Fig. 7. Graph summarising n-Gd_2O_3 and e-Gd_2O_3 models with similar reactivity characteristics in fuels with different ^{235}U enrichment levels: (a) matches with similar peak reactivity behaviour and (b) matches with equal highest reactivity rates.

Considering patterns in Fig. 7, two different equations were obtained to estimate the approximate e-Gd_2O_3 level in the assembly that will provide a similar behaviour to n-Gd_2O_3 when considering: the assembly's peak reactivity behaviours match (in Eq. 4), and when the assembly's highest reactivity rate (in Eq. 5).

$$M1_{e-Gd_2O_3} = 0.2917 \times M_{n-Gd_2O_3} \quad \text{(Eq. 4)}$$

$$M2_{e-Gd_2O_3} = 0.4167 \times M_{n-Gd_2O_3} \quad \text{(Eq. 5)}$$

Where $M_{n-Gd_2O_3}$ is the mass of n-Gd_2O_3, $M1_{e-Gd_2O_3}$ is the mass of e-Gd_2O_3 required to match peak reactivity with n-Gd_2O_3, and $M2_{e-Gd_2O_3}$ is the mass of e-Gd_2O_3 required to match highest reactivity with n-Gd_2O_3.

3.2.2. Depletion behaviour of Gd isotopes

Fig 8 shows the Gd isotope depletion behaviour of the 1.55 wt.% e-Gd_2O_3, and 6 wt.% n-Gd_2O_3, reported in Fig 5. The ^{157}Gd isotopes in e-Gd_2O_3 are depleted faster than the ^{155}Gd in n-Gd_2O_3. Similar behaviour was detected for all comparable e-Gd_2O_3/n-Gd_2O_3 systems (i.e. those reported in Fig. 5).

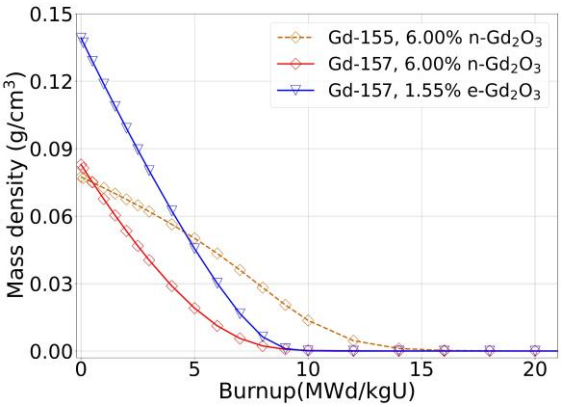

Fig. 8 Depletion of ^{155}Gd and ^{157}Gd isotopes in model has 1.55 wt.% e-Gd_2O_3, and 6.00 wt.% n-Gd_2O_3.

The averaged depletion behaviour of ^{155}Gd and ^{157}Gd isotopes in n-Gd_2O_3 (see Fig A6a and A6b) and ^{157}Gd isotopes in e-Gd_2O_3 (see Fig A6c) for 24 BA rods in models with 4.00 wt.% n-Gd_2O_3 and 1.10 wt.% e-Gd_2O_3 were exterminated. The results show that, the effect of self-shielding on the depletion of Gd isotopes is clear because, as expected, both ^{155}Gd and ^{157}Gd isotopes are depleted at the pellet surface faster than at the pellet centre.

3.2.3. Breeding behaviour of ^{239}Pu isotopes

To understand if the inclusion of e-Gd_2O_3 in the assembly could impact the breeding of ^{239}Pu, potentially providing a benefit to k_{inf}, the formation of ^{239}Pu is considered and compared to designs with n-Gd_2O_3. Fig. 9 shows the delta-^{239}Pu functions obtained by comparing the three chosen models against the reference assembly model without BA rods.

It was shown that in the well-moderated and homogeneous geometry of a PWR, an increase in ^{239}Pu results from an increase in BA within the assembly with both n-Gd_2O_3 and e-Gd_2O_3. In addition, the use of e-Gd_2O_3 promoted more ^{239}Pu breeding when compared to n-Gd_2O_3, which exhibits similar reactivity properties. It is also clear that models matched with n-Gd_2O_3 according to the equal highest reactivity caused higher ^{239}Pu breeding than models matched with similar peak reactivity behaviour. The increase in ^{239}Pu may provide additional reactivity during operation, thus contributing towards the higher k_{inf} later in life in the e-Gd_2O_3 assemblies.

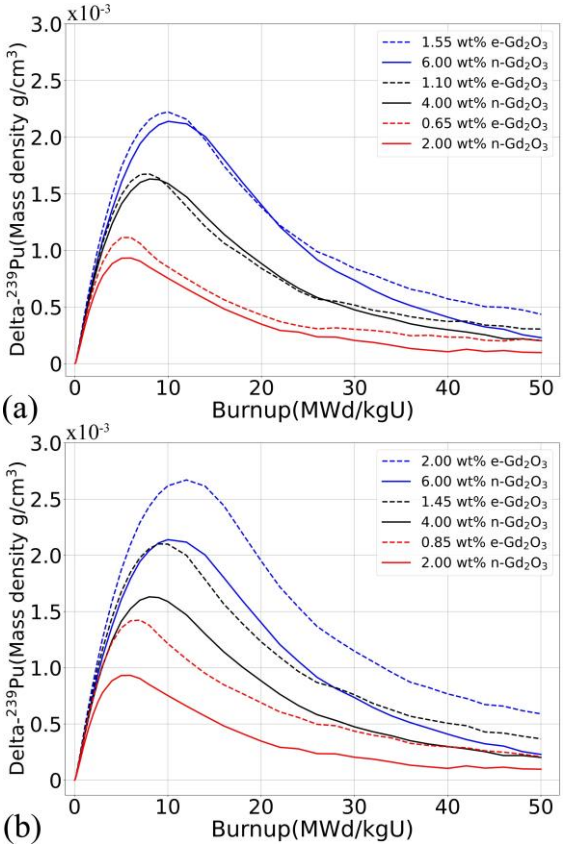

Fig. 9. Excess ^{239}Pu breeding (a) with n-Gd_2O_3 and e-Gd_2O_3 matches with similar peak reactivity behaviour and, (b) with n-Gd_2O_3 and e-Gd_2O_3 matches with equal highest reactivity rates, as compared with the reference without BA.

As is expected, a higher burnup was obtained on the pellet surface than the centre in fuel rods with BA due to self-shielding effects. Following this, the ^{239}Pu mass density measurements were taken from BA rods with 4.00 wt.% n-Gd_2O_3 and 1.25 wt.% e-Gd_2O_3 to determine if the use of e-Gd_2O_3 caused any changes to ^{239}Pu breeding behaviour within the fuel pellets. It was shown that e-Gd_2O_3 does not cause significant changes (see Fig. A7), and in both fuel models the amount of ^{239}Pu increases from the pellet centre towards the pellet surface and peaks at the surface.

3.4. Cost assessment

The matching set of models that have similar peak reactivity behaviour (see Figs. 5a, 5b and 5c), equal highest reactivity rates (see Figs. 5d, 5e and 5f) were evaluated from an economic perspective. Since the use of e-Gd_2O_3 enables use of more UO_2 in the fuel composition, there is an increase in fuel cost in all components directly or indirectly related to uranium (i.e. the cost of uranium, conversion, and enrichment). For the nominal costs, while the highest component cost for all models is cost of uranium enrichment, the lowest is purchasing the BA.

Comparing the costs for the set with the lowest additions of Gd_2O_3 with 2.00 wt.% n-Gd_2O_3 and 0.65 wt.% e-Gd_2O_3 (see Table A5), each assembly containing e-Gd_2O_3 is nominally ~ 6.1 kUSD more expensive than the model with n-Gd_2O_3 (this cost varies between ~4.1 kUSD and ~10 kUSD). For the models with 4.00 wt.% n-Gd_2O_3 and 1.10 wt.% e-Gd_2O_3 (see Table A6), each assembly containing e-Gd_2O_3 is nominally ~11.5 kUSD more expensive than those with n-Gd_2O_3 (this cost varies between ~7.7 kUSD and ~19.4 kUSD). For the models with 6.00 wt.% n-Gd_2O_3 and 1.55 wt.% e-Gd_2O_3 (see Table A7), each assembly containing e-Gd_2O_3 is nominally ~16.8 kUSD more expensive than those with n-Gd_2O_3 and this cost varies between ~11.1 kUSD and ~28.6 kUSD depending on the lowest and highest unit prices in the sensitivity range.

On the other hand, comparing the costs for models with 2.00 wt.% n-Gd_2O_3 and 0.85 wt.% e-Gd_2O_3 (see Table A8), each assembly containing e-Gd_2O_3 is nominally ~ 6.9 kUSD more expensive than those with n-Gd_2O_3 (this cost varies between ~4.5 kUSD and ~10.9 kUSD). For the models with 4.00 wt.% n-Gd_2O_3 and 1.45 wt.% e-Gd_2O_3 (see Table A9), each assembly containing e-Gd_2O_3 is nominally ~12.8 kUSD more expensive than those with n-Gd_2O_3 (this cost varies between ~8.7 kUSD and ~20.7 kUSD). For the models with 6.00 wt.% n-Gd_2O_3 and 2.00 wt.% e-Gd_2O_3 (see Table A10), each assembly containing e-Gd_2O_3 is nominally ~18.5 kUSD more expensive than the model has n-Gd_2O_3 and this cost varies between ~12.5 kUSD and ~30.0 kUSD depending on the lowest and highest unit prices in the sensitivity range.

The benefits of the e-Gd2O3 with respect to the integral reactivity is clear for the cases presented in Fig 5a-c and e. In addition to this benefit, there is an additional performance improvement when considering the mid-cycle and end of life reactivity compared to n-Gd_2O_3 in all cases in Fig 5. The reactivity benefit at the end of life can be estimated in terms of an extension of burnup for a given reactivity. For example, in Figure 5f, at a reactivity of kinf=1.1, the e-Gd_2O_3 has a larger burnup value of 23.9 MWd/kgU vs 22.9 MWd/kgU (equivalent to 2%). This 2% increase over the lifetime of a fuel (typically 54 months) equates to approximately 33 days of excess operation. Even though the assembly cost is ~18.5kUSD higher than the n-Gd_2O_3 assembly, this will manifest as an improvement to fuel cycle cost when considered in further full core analysis. Applying the same scenario with fuel models given in Fig 5d, with the use of e-Gd_2O_3 instead of n-Gd_2O_3, an extension of 0.7%, roughly equating to 11 days over its reactor residence period, more than making up for its small increase in cost per assembly of ~6.9kUSD and benefiting the overall levelized cost of electricity (LCOE). Further work building upon these results will be carried out considering the full core, multi-cycle behaviour.

4. Conclusion

The operational effect of Gd_2O_3 enriched with ^{157}Gd isotopes has been studied. The impact of e-Gd_2O_3 compared to n-Gd_2O_3 has been assessed with respect to reactivity, depletion behaviour of BA and ^{239}Pu breeding. Some preliminary economic assessments have also been carried out to guide future studies incorporating full-core analysis. The conclusions from this study are as follows:

- In agreement with previous work(Renier and Grossbeck, 2001), utilizing e-Gd_2O_3 can provide a similar reactivity behaviour to n-Gd_2O_3 whilst using a smaller volume of BA. Thus, because a lower proportion of Gd_2O_3 will be added to the fuel composition, lower proportion of UO_2 is displaced from the fuel providing higher reactivity.
- Also, in agreement with previous work(Renier and Grossbeck, 2001), the use of e-Gd_2O_3 provides a reduction in the amount of Gd isotopes that cause residual reactivity, from the fuel matrix, resulting in cleaner burn of the BA in fuel.
- Pairing the n-Gd_2O_3 and e-Gd_2O_3 by correlating peak reactivity behaviour, the use of e-Gd_2O_3 allows to obtain higher reactivity than n-Gd_2O_3. The amount of gained-reactivity rises significantly with the increase in n-Gd_2O_3 / e-Gd_2O_3 ratio.
- Pairing the n-Gd_2O_3 and e-Gd_2O_3 when considering the equal highest reactivity, e-Gd_2O_3 provides the same total reactivity only with high proportions of BA in the fuel composition.
- At high Gd contents, e-Gd_2O_3 is found to outperform n-Gd_2O_3 in terms of reactivity gains over the irradiation life of the fuel also in the case with equal highest reactivity; this provides a means for designing modern fuel assemblies for high burnup duty.
- Depletion of BA isotopes in the fuel is prevented as a result of the self-shielding effect, which is exacerbated by the increase of ^{235}U increasing the amount of neutron absorbing atoms in the fuel composition as a result of using e-Gd_2O_3.
- The rate of ^{239}Pu breeding reaches highest concentration where BA isotopes are depleted and the e-Gd_2O_3 produces a slightly higher amount of ^{239}Pu than the n-Gd_2O_3 ratio. In addition, the amount of ^{239}Pu increases from the centre of the fuel pellet to its surface and this increase shows an expected peak at the surface. The slight increase in ^{239}Pu content may provide an additional increase in k_{inf} during operation of fuel containing e-Gd_2O_3.
- In the scenarios considered, the use of e-Gd_2O_3 increases the cost of the assembly due to the cost of enrichment process of Gd_2O_3 but predominantly as a result of the increased use of

UO_2 in fuel composition. Also, the use of e-Gd_2O_3 can promote the acquisition of the reactivity properties exhibited by n-Gd_2O_3, with lower enrichment of uranium. Savings may be possible if using e-Gd_2O_3 to lower the enrichment of ^{235}U in fresh fuel as previously discussed by (Yilmaz, 2005).

- In this context, the number of effective full power days of reactor operation can be increased due to the increase in k_{inf} in a number of the scenarios considered. Thus, the total fuel cycle duration can be prolonged with the use of e-Gd_2O_3.

Further work, using 3D core analysis of the full reactor, is necessary to determine shutdown and thermal margins, as well as to calculate the levelized cost of electricity for the fuel cycle or plant lifetime for estimation of a realistic profit margins, but this study highlights the potential economic and performance benefits that moving towards e-Gd_2O_3 can provide.

Acknowledgements

The authors would like to thank, Ministry of National Education of the Turkish Republic. SCM, MD and WEL are funded through the Sêr Cymru II programme by Welsh European Funding Office (WEFO) under the European Development Fund (ERDF). We also acknowledge the support from the VTT Technical Research Centre of Finland and the OECD NEA Data Bank for providing access to Serpent 2. We also acknowledge the BEIS funded Advanced Fuel Cycle Programme led by NNL for their contribution and Dave Goddard is especially thanked for his support. In this study, all calculations were made on Supercomputing Wales.

References

Asou, M., Porta, J., 1997. Prospects for poisoning reactor cores of the future. Nucl. Eng. Des. 168, 261–270. https://doi.org/10.1016/s0029-5493(96)01322-2

Bejmer, K.H., Seveborn, O., 2004. Enriched Gadolinium as Burnable Absorber for PWR. Proc. PHYSOR Phys. Fuel Cycles Adv. Nucl. Syst. - Glob. Dev.

Dalle, H.M., Mattos, J.R.L. de, Dias, M.S., 2013. Enriched Gadolinium Burnable Poison for PWR Fuel – Monte Carlo Burnup Simulations of Reactivity, in: Current Research in Nuclear Reactor Technology in Brazil and Worldwide. https://doi.org/10.5772/53381

Durazzo, M., Freitas, A.C., Sansone, A.E.S., Ferreira, N.A.M., de Carvalho, E.F.U., Riella, H.G., Leal Neto, R.M., 2018. Sintering behavior of UO2–Er2O3 mixed fuel. J. Nucl. Mater. 510, 603–612. https://doi.org/10.1016/j.jnucmat.2018.08.051

Forsberg, C.W., 2011. The Future of the Nuclear Fuel Cycle, MIT.

Franceschini, F., Petrović, B., 2009. Fuel with advanced burnable absorbers design for the IRIS reactor core: Combined Erbia and IFBA. Ann. Nucl. Energy 36, 1201–1207. https://doi.org/10.1016/j.anucene.2009.04.005

Frybortova, L., 2019. VVER-1000 fuel cycles analysis with different burnable absorbers. Nucl. Eng. Des. 351, 167–174. https://doi.org/10.1016/j.nucengdes.2019.05.026

Galahom, A.A., 2017. Study of the possibility of using Europium and Pyrex alloy as burnable absorber in PWR. Ann. Nucl. Energy 110, 1127–1133. https://doi.org/10.1016/j.anucene.2017.08.052

Galahom, A.A., 2016. Investigation of different burnable absorbers effects on the neutronic characteristics of PWR assembly. Ann. Nucl. Energy 94, 22–31. https://doi.org/10.1016/j.anucene.2016.02.025

IAEA, 1995. Characteristics and Use of Urania-Gadolinia Fuels 1–191.

Kardoulaki, E., White, J.T., Byler, D.D., Frazer, D.M., Shivprasad, A.P., Saleh, T.A., Gong, B., Yao, T., Lian, J., McClellan, K.J., 2020. Thermophysical and mechanical property assessment of UB2 and UB4 sintered via spark plasma sintering. J. Alloys Compd. 818, 153216. https://doi.org/10.1016/j.jallcom.2019.153216

Ko, W. Il, Gao, F., 2012. Economic analysis of different nuclear fuel cycle options. Sci. Technol. Nucl. Install. 2012. https://doi.org/10.1155/2012/293467

Leppänen, J., Pusa, M., Viitanen, T., Valtavirta, V., Kaltiaisenaho, T., 2015. The Serpent Monte Carlo code: Status, development and applications in 2013. Ann. Nucl. Energy 82, 142–150. https://doi.org/10.1016/j.anucene.2014.08.024

Middleburgh, S., Bolukbasi, M., Goddard, D., 2020. Enhancing economics with ATF. Nucl. Eng. Int. Mag. 24–27.

Nuclear Regulatory Commission, 2011. Westinghouse AP1000 Design Control Document Rev. 19- Tier 2 Chapter 4.

Oprea, C., Oprea, A., 2014. Cross sections of Gadolinium isotopes in neutron transmission simulated experiments with low energy neutrons up to 100 eV. https://doi.org/10.13140/RG.2.1.4373.5122

Ozer, O., Edsinger, K., 2006. Optimum Cycle Length and Discharge Burnup for Nuclear Fuel Phase II : Results Achievable with Enrichments Greater than 5 w / o 3.

Pagano, L., Valença, G.P., Silva, S.L., Cláudio, A.E.L., Ivashita, F.F., Barco, R., de Medeiros, S.N., Paesano, A., 2008. Mössbauer study and structural characterization of UO2-Gd2O3 sintered compounds. J. Nucl. Mater. 378, 25–29. https://doi.org/10.1016/j.jnucmat.2008.03.024

Qin, M.J., Middleburgh, S.C., Cooper, M.W.D., Rushton, M.J.D., Puide, M., Kuo, E.Y., Grimes, R.W., Lumpkin, G.R., 2020. Thermal conductivity variation in uranium dioxide with gadolinia additions. J. Nucl. Mater. 540, 152258. https://doi.org/10.1016/j.jnucmat.2020.152258

Reda, S.M., Mustafa, S.S., Elkhawas, N.A., 2020. Investigating the Performance and safety features of Pressurized water reactors using the burnable poisons. Ann. Nucl. Energy 141, 107354. https://doi.org/10.1016/j.anucene.2020.107354

Renier, J.-P.A., Grossbeck, M.L., 2001. Development of Improved Burnable Poisons for Commerical Nuclear Power Reactors.

Sanders, C.E., Wagner, J.C., 2002. Study of the Effect of Integral Burnable Absorbers for PWR Burnup Credit, Ornl/Tm-2000/321.

Santala, M.I.K., Daavittila, A.S., Lauranto, H.M., Salomaa, R.R.E., 1997. Odd-isotope enrichment studies of Gd by double resonance laser-ionization for the production of burnable nuclear reactor poison. Appl. Phys. B Lasers Opt. 64, 339–347. https://doi.org/10.1007/s003400050182

Schlieck, M., Berger, H.D., Neufert, A., 2001. Optimized gadolinia concepts for advanced in-core fuel management in PWRs. Nucl. Eng. Des. 205, 191–198. https://doi.org/10.1016/S0029-5493(00)00355-1

Simmons, R.L., Jones, N.D., Popa, F.D., Mueller, D.E., Pritchett, J.E., 1988. Integral Fuel Burnable Absorbers with ZrB2 in Pressurized Water Reactors. Nucl. Technol. 80, 343–348. https://doi.org/10.13182/NT88-A34058

The Economics of the Nuclear Fuel Cycle, 1994. , Nuclear Energy Agency, Organisation for Economic Co-Operation and Development.

Tran, H.N., Hoang, H.T.P., Liem, P.H., 2017. Feasibility of using Gd2O3 particles in VVER-1000 fuel assembly for controlling excess reactivity. Energy Procedia 131, 29–36. https://doi.org/10.1016/j.egypro.2017.09.442

U.S. department of Energy, 2017. Advanced Fuel Cycle Cost Basis – 2017 Edition.

Uguru, E.H., Sani, S.F.A., Khandaker, M.U., Rabir, M.H., Karim, J.A., 2020. A comparative study on the impact of Gd2O3 burnable neutron absorber in UO2 and (U, Th)O2 fuels. Nucl. Eng. Technol. 52, 1099–1109. https://doi.org/10.1016/j.net.2019.11.010

Yilmaz, S., 2005. Multi Level Optimization of Burnable Poison Utilization for Advanced PWR Fuel Management. The Pennsylvania State University.

Yilmaz, S., Ivanov, K., Levine, S., Mahgerefteh, M., 2006. Development of enriched Gd-155 and Gd-157 burnable poison designs for a PWR core. Ann. Nucl. Energy 33, 439–445. https://doi.org/10.1016/j.anucene.2005.11.011

Appendix A

Fuel densities used in simulations are shown in Table A1.

Table A1. Fuel densities (wt.%)

Fuel Composition	Density (gr/cm^3)
3 wt.% ^{235}U	10.408
4 wt.% ^{235}U	10.407
5 wt.% ^{235}U	10.406
6 wt.% ^{235}U	10.404
4 wt.% ^{235}U + 2.00 wt.% n-Gd_2O_3	10.341
5 wt.% ^{235}U + 1.00 wt.% n-Gd_2O_3	10.373
5 wt.% ^{235}U + 2.00 wt.% n-Gd_2O_3	10.340
5 wt.% ^{235}U + 4.00 wt.% n-Gd_2O_3	10.273
5 wt.% ^{235}U + 6.00 wt.% n-Gd_2O_3	10.207
6 wt.% ^{235}U + 2.00 wt.% n-Gd_2O_3	10.338
5 wt.% ^{235}U + 0.65 wt.% e-Gd_2O_3	10.384
5 wt.% ^{235}U + 0.85 wt.% e-Gd_2O_3	10.378
5 wt.% ^{235}U + 1.00 wt.% e-Gd_2O_3	10.373
5 wt.% ^{235}U + 1.10 wt.% e-Gd_2O_3	10.369
5 wt.% ^{235}U + 1.45 wt.% e-Gd_2O_3	10.358
5 wt.% ^{235}U + 1.55 wt.% e-Gd_2O_3	10.354
5 wt.% ^{235}U + 2.00 wt.% e-Gd_2O_3	10.340

Fuel assembly designs used in simulations are given in Fig. A.1 and Fig. A.2.

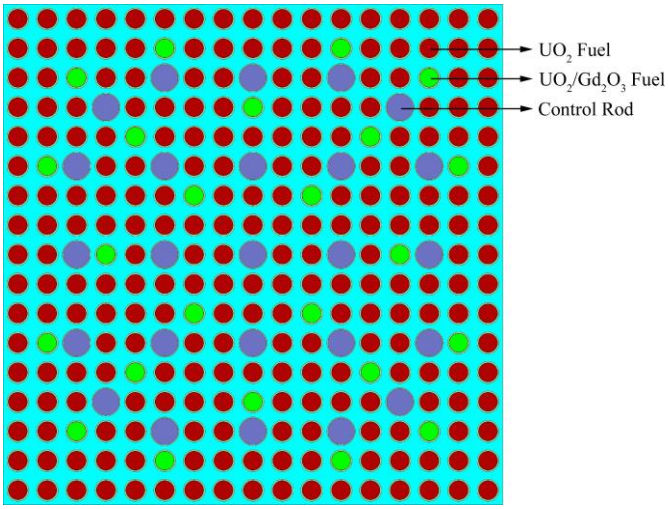

Fig. A1 Assembly 1 (24 BA rods) (Reda *et al.*, 2020)

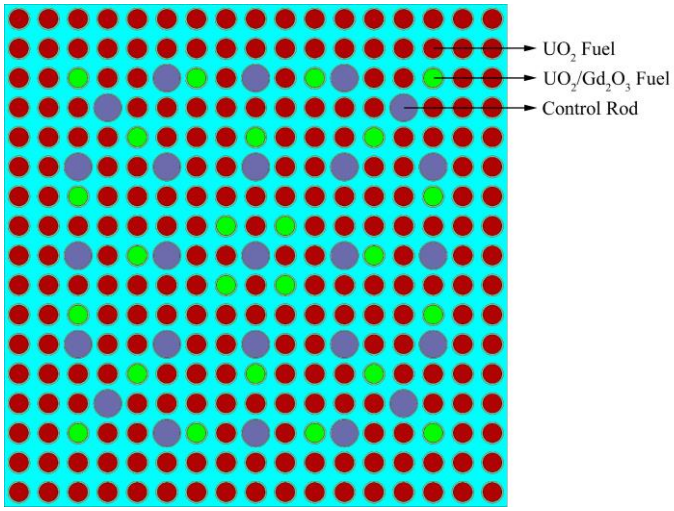

Fig. A2 Assembly 2 (24 BA rods) (Uguru *et al.*, 2020)

Fuel rod design used in simulations is shown in Fig. A3.

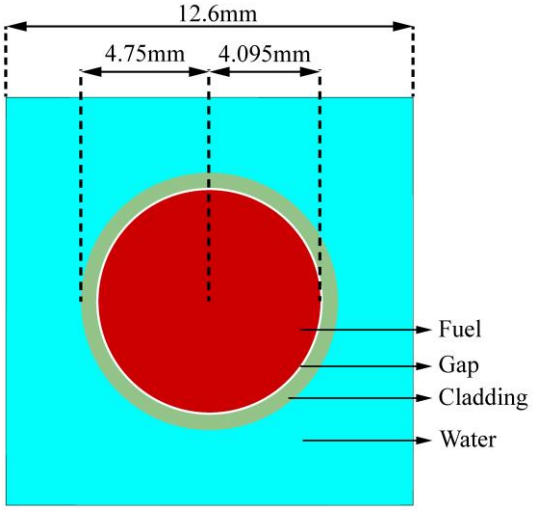

Fig A1. Fuel rod cross section

Unit prices used for fuel cost calculation are shown in Table A2.

Table A2. Unit prices for each component (Asou and Porta, 1997; U.S. department of Energy, 2017; Yilmaz, 2005)

Type of component	Unit Prices		
	Low	Nominal	High
uranium \$/lb U_3O_8	13.1	33.1	114
conversion \$/kg	6.5	13	19
Uranium enrichment \$/SWU	97	128	154
fabrication \$/kg	230	400	575
Gd_2O_3 \$/kg*	255	397	516
^{157}Gd enrichment \$/g*	7,4	10	13.6

* High and low unit costs were obtained by assuming that the nominal cost regularly increased and decreased by average USA escalation rate in the period from the year it was stated in the literature to 2020.

Equations used for fuel cost calculation are as follows(*The Economics of the Nuclear Fuel Cycle*, 1994) and the parameters are given in Table A3.

Cost of uranium

$$F_1 = M_f \times f_1 \times P_1 \times (1 + S_1)^{t-t_b} \quad \text{(Eq. A1)}$$

where:

$$M_f = \frac{e_p - e_t}{e_f - e_t} \times M_p \quad \text{(Eq. A2)}$$

$$f_1 = (1 + l2) \times (1 + l3) \times (1 + l4) \quad \text{(Eq. A3)}$$

From all front-end components:

$$t = t_c - t_b \quad \text{(Eq. A4)}$$

Cost of conversion

$$F_2 = M_f \times f_2 \times P_2 \times (1 + S_2)^{t-t_b} \quad \text{(Eq. A5)}$$

where:

$$f_2 = (1 + l2) \times (1 + l3) \times (1 + l4) \quad \text{(Eq. A6)}$$

Cost of enrichment

$$F_3 = SWU \times f_3 \times P_3 \times (1 + S_3)^{t-t_b} \quad \text{(Eq. A7)}$$

where:

$$SWU = M_p V_p + M_t V_t - M_f V_f \quad \text{(Eq. A8)}$$

$$M_t = M_f - M_p \quad \text{(Eq. A9)}$$

$$V_x = (2e_x - 1) \times \ln \frac{e_x}{(1 - e_x)} \quad \text{(Eq. A9)}$$

x is subscript for f, p or t

$$f_3 = (1 + l3) \times (1 + l4) \quad \text{(Eq. A10)}$$

Cost of fabrication

$$F_4 = M_f \times f_4 \times P_4 \times (1 + S_4)^{t-t_b} \quad \text{(Eq. A11)}$$

where:

$$f_4 = (1 + l4) \quad \text{(Eq. A12)}$$

Table A3. Parameter notation for fuel cost calculations

Time	t
Base date of monetary unit	t_b
Date of fuel loading	t_c
Mass of uranium feed (kg)	M_f
Mass of uranium charged in reactor (kg)	M_p
Mass of uranium in the tails (kg)	M_t
Fraction of ^{235}U in the uranium feed	e_f (0.711%)
Fraction of ^{235}U charged in reactor	e_p
Fraction of ^{235}U in the tails	e_t
Conversion factor from kg U to lb U^3O^8 (a lb U3O8 per kg U)	a (2.6)
Total component cost	F_i
Unit cost	P_i
Escalation rate	s_i
Material losses	l_i
Total loss factor	f_i
Lead or lag time	t_i

Where:

i = 1 Uranium purchase — P_1 = Monetary units per lb U_3O_8

i = 2 Conversion — P_2 = Monetary units per kg U

i = 3 Enrichment — P_3 = Monetary units per SWU

i = 4 Fabrication — P_4 = Monetary units per kg U

Fuel cycle data used for fuel cost calculation are shown in Table A4.

Table A4. Fuel cycle data (Forsberg, 2011; *The Economics of the Nuclear Fuel Cycle*, 1994)

Lead time of uranium purchase	24 months
Lead time of conversion	18 months
Lead time of Uranium enrichment	12 months
Lead time of fabrication	6 months
Material loss during conversion (%)	0.2
Material loss during enrichment (%)	0.2
Material loss during fabrication (%)	0.2
Tails assay (%)	0.25
Escalation rate (1.9)	1.9

Depletion behaviours for ^{155}Gd and ^{157}Gd isotopes of models with different ^{235}U enrichment levels are shown in Fig A4.

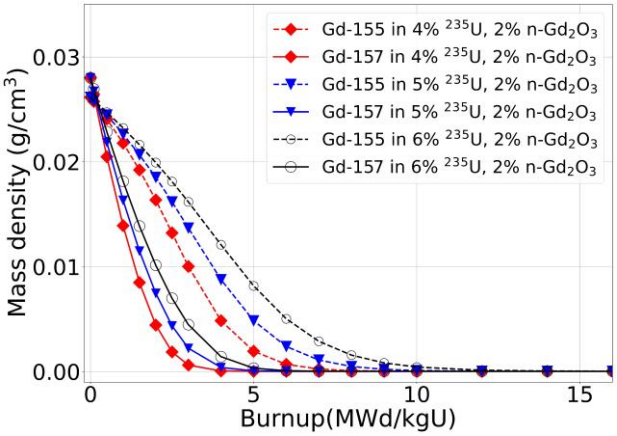

Fig. A4. Depletion of ^{155}Gd and ^{157}Gd isotopes in models have 2.00 wt.% n-Gd_2O_3 and different ^{235}U enrichment levels

Accumulated reactivity gain, provided by e-Gd_2O_3 over n-Gd_2O_3 with increasing average fuel burnup to 50MWe/kgU, of the models reported in Fig. 5 are shown in Fig. A5.

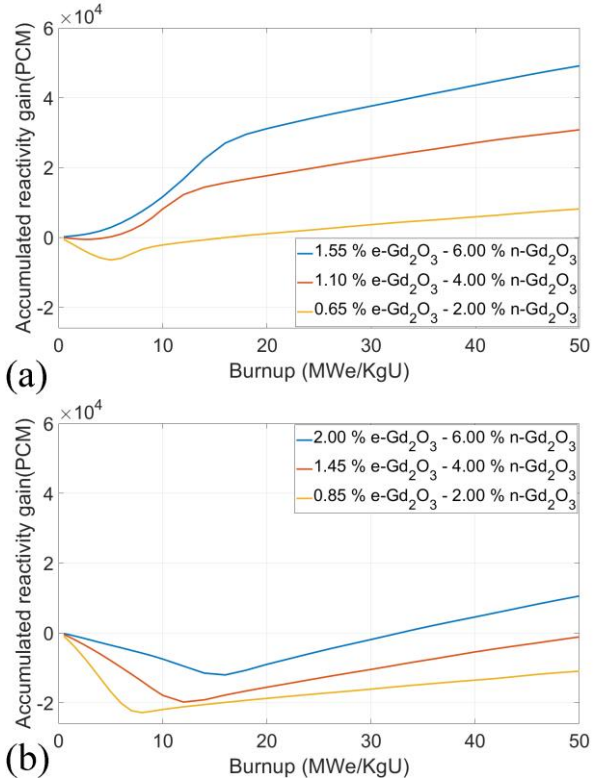

Fig. A5 - Accumulated reactivity gain provided by e-Gd_2O_3 over n-Gd_2O_3 with increasing average fuel burnup to 50MWe/kgU for (a) matches with similar peak reactivity behaviours (b) matches with equal highest reactivity rates (c) matches with equal highest reactivity rates

Fig. 6A shows the depletion behaviour of Gd isotopes from the centre to the surface of the fuel pellets with BA.

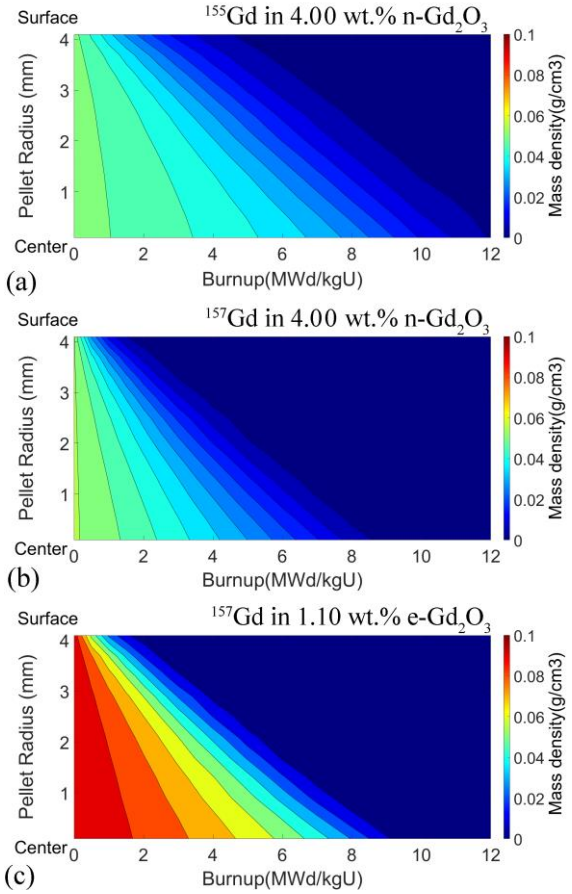

Fig. A6. Depletion rates of (a) ^{155}Gd in 4.00 wt.% n-Gd_2O_3, (b) ^{157}Gd in 4.00 wt.% n-Gd_2O_3 and (c) ^{157}Gd in 1.25 wt.% e-Gd_2O_3.

Fig. 7A shows the ^{239}Pu breeding behaviour in the assembly from the centre to the surface of the pellets.

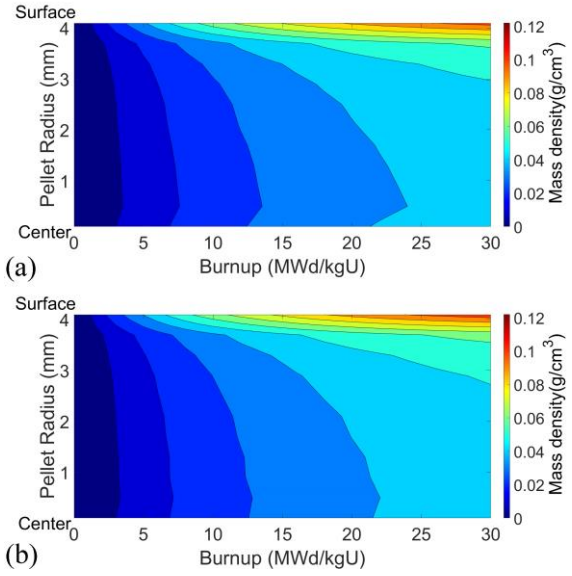

Fig. A7. Total ^{239}Pu breeding assemblies of models with (a) 4.00 wt.% n-Gd_2O_3, and (b) 1.25 wt.% e-Gd_2O_3.

Table A5. Single assembly fuel cost comparison of models with 2.00 wt.% n-Gd_2O_3, and 0.65 wt.% e-Gd_2O_3 both in 5 wt.% ^{235}U (all values are provided in kUSD).

	2.00 wt.% n-Gd_2O_3			0.65 wt.% e-Gd_2O_3		
	Low	Nominal	High	Low	Nominal	High
Cost of uranium	221.64	560.03	1,928.81	222.00	560.93	1,931.90
Cost of conversion	42.70	85.40	124.81	42.77	85.53	125.01
Cost of enrichment	493.64	651.40	783.71	494.43	652.44	784.97
Cost of fabrication	148.54	258.38	371.62	148.97	259.09	372.51
Cost of Gd_2O_3	0.28	0.44	0.58	0.09	0.14	0.19
Cost Of ^{157}Gd enrichment	0.00	0.00	0.00	2.69	3.64	4.95
Cost of total fuel for assembly	906.80	1,555.65	3,209.39	910.95	1,561.79	3,219.49
Cost difference to				4,15	6,14	10,01

Table A6. Single assembly fuel cost comparison of models have 4.00 wt.% n-Gd_2O_3, and 1.10 wt.% enriched Gd_2O_3 both in 5 wt.% ^{235}U (all values are provided in kUSD).

	4.00 wt.% n-Gd_2O_3			1.10 wt.% e-Gd_2O_3		
	Low	Nominal	High	Low	Nominal	High
Cost of uranium	221.12	558.70	1,924.23	221.88	560.63	1,930.86
Cost of conversion	42.60	85.19	124.51	42.74	85.49	124.94
Cost of enrichment	492.46	649.85	781.85	494.16	652.09	784.55
Cost of fabrication	147.90	257.33	370.30	148.83	258.86	372.21
Cost of Gd_2O_3	0.57	0.88	1.14	0.16	0.24	0.32
Cost Of ^{157}Gd enrichment	0.00	0.00	0.00	4.55	6.15	8.37
Cost of total fuel for assembly	904.65	1,551.95	3,201.77	912.32	1,563.46	3,221.18
Cost difference				7.67	11.51	19.41

Table A7. Single assembly fuel cost comparison of models have 6.00 wt.% n-Gd_2O_3, and 1.55 wt.% e-Gd_2O_3 both in 5 wt.% ^{235}U (all values are provided in kUSD).

	6.00 wt.% n-Gd_2O_3			1.55 wt.% e-Gd_2O_3		
	Low	Nominal	High	Low	Nominal	High
Cost of uranium	220.60	557.39	1,919.71	221.76	560.33	1,929.83
Cost of conversion	42.50	84.99	124.22	42.72	85.44	124.88
Cost of enrichment	491.31	648.32	780.01	493.90	651.74	784.12
Cost of fabrication	147.28	256.29	368.99	148.68	258.62	371.91
Cost of Gd_2O_3	0.84	1.31	1.70	0.22	0.34	0.45
Cost Of ^{157}Gd enrichment	0.00	0.00	0.00	6.41	8.66	11.78
Cost of total fuel for assembly	902.52	1,548.31	3,194.25	913.69	1,565.13	3,222.86
Cost difference				11.17	16.82	28.61

Table A8. Single assembly fuel cost comparison of models have 2.00 wt.% n-Gd_2O_3, and 0.85 wt.% e-Gd_2O_3 both in 5 wt.% ^{235}U (all values are provided in kUSD).

	2.00 wt.% n-Gd_2O_3			0.85 wt.% e-Gd_2O_3		
	Low	Nominal	High	Low	Nominal	High
Cost of uranium	221.64	560.03	1,928.81	221.95	560.80	1,931.45
Cost of conversion	42.70	85.40	124.81	42.76	85.51	124.98
Cost of enrichment	493.64	651.40	783.71	494.31	652.29	784.78
Cost of fabrication	148.54	258.38	371.62	148.91	258.99	372.38
Cost of Gd_2O_3	0.28	0.44	0.58	0.12	0.19	0.25
Cost Of ^{157}Gd enrichment	0.00	0.00	0.00	3.52	4.76	6.47
Cost of total fuel for assembly	906.80	1,555.65	3,209.39	911.57	1,562.54	3,220.26
Cost difference to				4.47	6.89	10.87

Table A9. Single assembly fuel cost comparison of models have 4.00 wt.% n-Gd_2O_3, and 1.45 wt.% e-Gd_2O_3 both in 5 wt.% ^{235}U (all values are provided in kUSD).

	4.00 wt.% n-Gd_2O_3			1.45 wt.% e-Gd_2O_3		
	Low	Nominal	High	Low	Nominal	High
Cost of uranium	221.12	558.70	1,924.23	221.79	560.40	1,930.07
Cost of conversion	42.60	85.19	124.51	42.73	85.45	124.89
Cost of enrichment	492.46	649.85	781.85	493.96	651.82	784.22
Cost of fabrication	147.90	257.33	370.30	148.71	258.67	371.98
Cost of Gd_2O_3	0.57	0.88	1.14	0.21	0.32	0.42
Cost Of ^{157}Gd enrichment	0.00	0.00	0.00	6.00	8.10	11.02
Cost of total fuel for assembly	904.65	1,551.95	3,201.77	913.39	1,564.77	3,222.50
Cost difference				8.74	12.82	20.73

Table A10. Single assembly fuel cost comparison of models have 6.00 wt.% n-Gd_2O_3, and 2.00 wt.% e-Gd_2O_3 both in 5 wt.% ^{235}U (all values are provided in kUSD).

	6.00 wt.% n-Gd_2O_3			2.00 wt.% e-Gd_2O_3		
	Low	Nominal	High	Low	Nominal	High
Cost of uranium	220.60	557.39	1,919.71	221.64	560.03	1,928.81
Cost of conversion	42.50	84.99	124.22	42.70	85.40	124.81
Cost of enrichment	491.31	648.32	780.01	493.64	651.40	783.71
Cost of fabrication	147.28	256.29	368.99	148.54	258.38	371.62
Cost of Gd_2O_3	0.84	1.31	1.70	0.28	0.44	0.58
Cost Of ^{157}Gd enrichment	0.00	0.00	0.00	8.26	11.16	15.17
Cost of total fuel for assembly	902.52	1,548.31	3,194.25	915.06	1,566.80	3,224.56
Cost difference				12.54	18.49	30.31